Effect of Viscosity on the Kinetics of α−Helix and β−Hairpin Formation

ARTICLE *in* THE JOURNAL OF PHYSICAL CHEMISTRY B · DECEMBER 2000

Impact Factor: 3.3 · DOI: 10.1021/jp0022048

3 AUTHORS, INCLUDING:

Gouri S. Jas
Central University of the Caribbean
44 PUBLICATIONS **1,824** CITATIONS

SEE PROFILE

Effect of Viscosity on the Kinetics of α-Helix and β-Hairpin Formation

Gouri S. Jas, William A. Eaton,* and James Hofrichter*

Laboratory of Chemical Physics, Building 5, National Institute of Diabetes and Digestive and Kidney Diseases, National Institutes of Health, Bethesda, Maryland 20892-0520

Received: June 16, 2000; In Final Form: August 23, 2000

Nanosecond laser temperature jumps and fluorescence detection were used to measure the effect of viscosity on the kinetics of α-helix and β-hairpin formation in peptides containing 21 and 16 amino acids, respectively. The solvent viscosity was changed by adding glucose and sucrose at concentrations that do not significantly alter the equilibrium unfolding curves. Analysis of the temperature dependence at fixed solvent compositions shows that the activation energies are also unaffected, indicating that the slowing of the relaxation rates upon addition of the sugars results entirely from their dynamical effect of increasing the solvent viscosity (η). The rate of β-hairpin formation was found to vary nearly as $1/\eta$, as predicted by Kramers theory in the high friction limit. In contrast, the rate of α-helix formation exhibited a fractional viscosity dependence ($k = \eta^{-\alpha}$) with an exponent $\alpha \approx 0.6$. The intrinsic activation energy for the elementary kinetic step of rotating a pair of backbone dihedral angles, obtained using a simple statistical mechanical model, is near zero for the β-hairpin but is ∼5 kcal/mol for the α-helix. If a higher barrier frequency can be associated with the larger activation energy, the fractional viscosity dependence for the α-helix may result from the fact that motion across the barrier top is faster than the solvent relaxation time.

Introduction

Understanding the mechanism of secondary structure formation is an essential ingredient to understanding how proteins fold.[1] With the relatively recent application of the laser-temperature jump technique,[2,3] it has been possible to investigate the kinetics of α-helix[4−7] and β-hairpin[8,9] formation in detail. Modeling these results indicates that the temperature dependence of the rates for the elementary kinetic steps is small.[5−9] An accurate determination of the magnitude of these energy barriers therefore requires subtracting the contribution to the observed temperature dependence which results from the change in solvent viscosity. Viscosity studies also introduce the possibility of acquiring new insights into the dynamics of secondary structure formation. Dihedral angle motions of the elementary steps in helix and hairpin formation are not unlike very fast photoisomerization reactions that have been studied extensively using time-resolved optical techniques with picosecond lasers.[10,11] There are also possible connections to nuclear magnetic resonance measurements of local backbone reorientational correlation times in homopolymers.[12] The rates for these processes are often found not to depend inversely on the first power of the viscosity (η), as predicted by Kramers theory in the high friction limit,[13] but to vary as $\eta^{-\alpha}$, where $0 < \alpha < 1$. The fractional viscosity dependence for both isomerization reactions and local backbone motions of homopolymers has generally been interpreted in terms of the theory of Grote and Hynes.[14] This extension of Kramers theory accounts for the fact that the friction encountered in crossing the barrier top depends on the time scale of this motion relative to the solvent viscoelastic relaxation time.

Studies on the viscosity dependence of the overall rates are also important because they may provide a new kind of test of molecular simulations of secondary structure formation. Just recently computational capability has developed to the point where it is possible to consider calculating a sufficiently large number of long trajectories to perform all-atom molecular dynamics simulations of the kinetics of α-helix and β-hairpin formation.[15] A substantial gain in computational speed is obtained when only the polypeptide atoms are explicitly considered and the dynamical effects of the solvent are included by using the Langevin equation. An important test of simulations with and without explicit solvent would be their ability to reproduce experimentally determined viscosity exponents.

In this work we have measured the viscosity dependence of the relaxation rates for both the 21-residue α-helix and the 16-reside β-hairpin used in our previous investigations (Figure 1).[6,8,9] Solvent viscosity was increased by the addition of glucose and sucrose to concentrations that do not alter the folding/unfolding equilibrium, as determined by circular dichroism and fluorescence measurements. Studies of the temperature dependence of the kinetics show that these viscogenic agents also do not alter the viscosity-corrected activation energies. Together these equilibrium and kinetic results suggest that the sugars do not significantly affect the energy surface, so that changes in rates result entirely from the effects of viscosity on the dynamics. We find that the relaxation rate for the β-hairpin varies nearly as the inverse first power of the solvent viscosity, as predicted by Kramers theory. In contrast, the helix relaxation rate shows a significantly smaller viscosity dependence, and can be explained by a power law in which the rate varies as $\eta^{-\alpha}$, where $\alpha \approx 0.6$. We discuss several interpretations of fractional viscosity dependence, including the breakdown of Stokes law relating the macroscopic solvent viscosity to the static friction, the effect of time-dependent friction, and the possible role of internal friction.

* Correspondence can be addressed to either author.

10.1021/jp0022048
Published on Web 12/07/2000

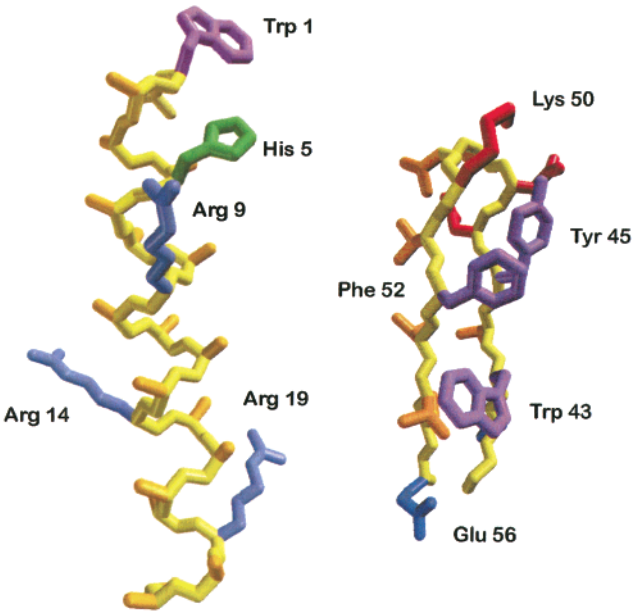

Figure 1. Structures of α-helix and β-hairpin. The structure of the α-helix was obtained after first constructing a helical structure using the sequence builder option in the graphics program "Quanta". To approximate the relative orientations of the tryptophan and protonated histidine side chains, 200 ps of molecular dynamics simulations was carried out in explicit water using CHARMM 24.[34] The β-hairpin structure was obtained from the coordinates of the full protein GB1 domain structure (Protein Data Bank file 1PGB).

Experimental Section

Materials. The sequence of the 21 residue α-helix-forming peptide is Ac−WAAAH$^+$(AAAR$^+$A)$_3$A-NH$_2$.[6] Acetylation and amidation remove the charges at the N- and C-termini, respectively. The sequence of the β-hairpin forming peptide is GEWTYDDATKTFTVTE, corresponding to residues 41−56 of protein GB1.[16] Both peptides were purchased from California Peptide Research, Inc. (Napa, CA), and were >95% pure. *N*-acetyl-L-tryptophanamide (NATA) was >99% pure and was purchased from Sigma. Peptide concentrations were determined from the optical absorbance at 280 nm, using extinction coefficients of 5690 M^{-1} cm^{-1} for the α-helical peptide[17] and 6970 M^{-1} cm^{-1} for the β-hairpin peptide.[8] Measurements on the β-peptide were made in 20 mM phosphate buffer at pH 7.2, while measurements on the α-peptide were made in 20 mM acetate buffer at pH 4.9 to ensure protonation of the histidine. In kinetic experiments the concentration of the peptides was 0.6−0.8 mM. Viscosities at 293 K for glycerol and ethylene glycol were obtained from values given in the *CRC Handbook of Chemistry and Physics* (55th edition, 1974). Viscosities of glucose and sucrose solutions in the temperature range 0−50 °C were obtained from measurements at Cannon Instrument Co. (State College, PA) of the density and kinematic viscosity using a capillary (Ubbelohde type) viscometer (Cannon Instrument Co.).

Equilibrium Experiments. Circular dichroism measurements were made with a Jasco 710 spectropolarimeter. Steady-state fluorescence spectra were measured with a SPEX "Fluorolog-2" spectrofluorometer (model F1T11I). Quantum yields are relative to NATA, taken as 0.13 at 293 K.[18]

Kinetic Experiments. The instrument used in the temperature jump experiments has been described in detail elsewhere.[3,5,6] The fundamental of a Q-switched Nd:YAG laser at 1064 nm was Raman-shifted in a high-pressure cell containing methane and helium to produce a ∼5 ns, ∼10 mJ pulse at 1540 nm. To obtain more uniform heating, the 1540 nm pulse was first split using a 50:50 beam splitter and focused onto the same spot from opposite sides of the sample (0.05 cm × 1 cm × 4.5 cm) cuvette. The delay between these two pulses was ∼5 ns, so the total duration of the heating pulses was ∼10 ns. The probe source for continuous excitation of tryptophan was an intracavity frequency doubled argon ion laser (Coherent "Innova" 300) operating at 264 nm. The fluorescence was filtered with 320−400 nm band-pass filter, collected at 90° with an end-on photomultiplier tube (Hamamatsu R6427), and recorded using a transient digitizer (Tektronix TDS 620). In a typical experiment temperature jumps of 10−12 K were obtained, and a single kinetic trace measured by averaging the curves from 3000 laser shots; the laser operated at 1.66 Hz to allow thermal diffusion out of the ∼0.5 mm to be completed prior to the next heating pulse. The temperature increase was determined by measuring the change in fluorescence of NATA at each initial temperature under identical experimental conditions before and after collecting data on the peptide. To minimize photodamage a shutter which remained open only during collection of a kinetic trace (∼5 ms), was inserted in front of the UV laser. To prevent cavitation, solutions were degassed by aspiration prior to being sealed in the cuvettes.

To fit the kinetic data, it is necessary to describe both the initial change in fluorescence intensity and the subsequent relaxation. It was assumed that the measured data could be described by a step change in fluorescence intensity which coincided with the change in sample temperature and a subsequent exponential relaxation to the final equilibrium fluorescence intensity. In practice, the fit was carried out by using two basis functions: one a step change from 0 to 1 at $t = 0$ and the other having a value of 1 at negative times and exponentially decaying to zero at positive times. These basis functions, calculated with a trial value for the relaxation time, were first convoluted with an instrument response function obtained from independent fits to kinetic traces of NATA fluorescence. The optimum amplitudes were then calculated using a linear least squares procedure in each iteration. In carrying out the fit, the residuals were calculated for a set of values for the $t = 0$ time point and the smallest residual was used in each iteration. Data points at times from 0 to 20 ns relative to $t = 0$ (about ±10 ns relative to the peak of the excitation pulse) were omitted in calculating the sum of squared residuals because a sharp negative spike can also be observed upon excitation of NATA and tryptophan in water.[6]

The measured progress curves were slightly distorted by a small step-increase in the fluorescence intensity, which occurred at ∼350 ns. The physical origin of this increase is unclear, but it may result from local inhomogeneity in the sample temperature. In any case, this fluorescence increase is unrelated to the change in the helix−coil equilibrium, since it also appears in experiments on NATA in water. For NATA this fluorescence increase could be fitted with a function which had the temporal profile of a squared Gaussian, with amplitudes which are about 1.5% of the overall change in fluorescence produced by the temperature jump. To estimate the uncertainty in the fitted rates which results from this effect, fits were also carried out including an additional basis function, having values of 0 at negative times and a squared Gaussian profile at positive times. In these fits the temporal position of the squared Guassian was optimized using nonlinear least squares and its amplitude optimized by linear least squares in each iteration.

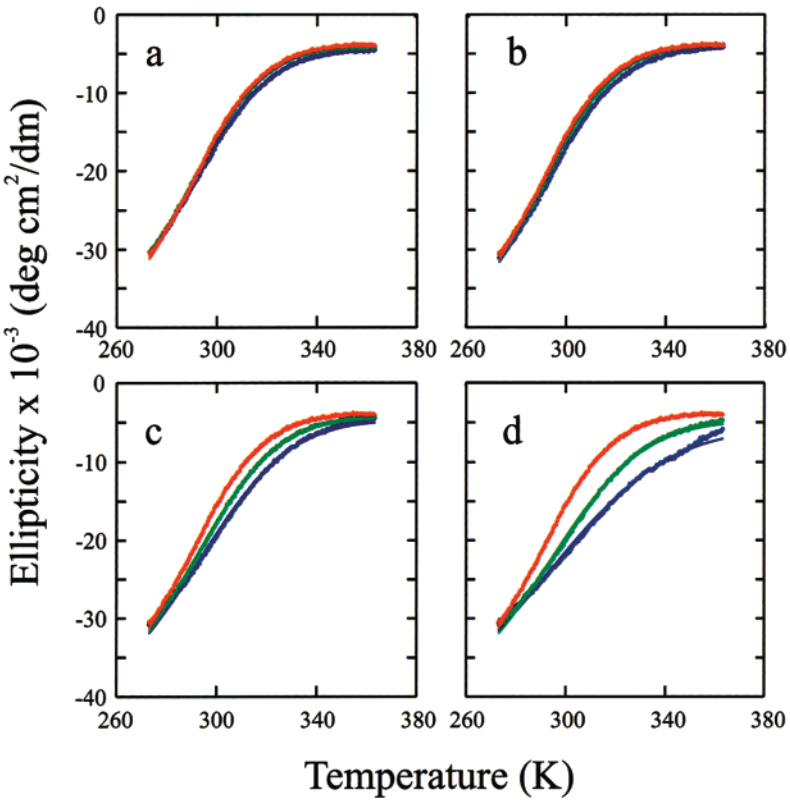

Figure 2. Thermal unfolding curves for 21-residue helix-forming peptide. The molar ellipticity at 220 nm is shown versus temperature for different concentrations of (a) glucose, (b) sucrose, (c) glycerol and (d) ethylene glycol. Melting curves are shown for (a) glucose concentrations of 1.08 M (green) and 1.7 M (blue), (b) sucrose concentrations of 0.63 M (green) and 0.92 M (blue), (c) glycerol concentrations of 2.5 M (green) and 4.0 M (blue), and (d) ethylene glycol concentrations of 4.0 m (green) and 7.0 M (blue). In each panel the melting curve in water (red) is shown for reference. The points are the data, while the thin, continuous curves were obtained by fitting the data with a two-state model. Except for the highest concentrations of glycerol and ethylene glycol, the fits are so good that the fitted curves are not visible.

Results

α-Helix Equilibrium Experiments. Our first objective was to find solvent systems in which the viscosity could be increased by an amount sufficient to establish the viscosity dependence of the kinetics without perturbing the helix−coil equilibrium. We therefore carried out a series of thermal unfolding curves using four well-known viscogenic agents—glycerol, ethylene glycol, sucrose, and glucose. Thermal unfolding was monitored by the circular dichroism at 220 nm, which provides a convenient and reliable measure of the fractional helix content (Figure 2). At concentrations that produce viscosities of ∼3 cP, glycerol and ethylene glycol markedly stabilize the helix. In contrast, concentrations of glucose and sucrose that increase the viscosity up to ∼3 cP produce very small changes in the unfolding curves. On the basis of these results, we chose to use these sugars in the kinetic studies.

To assess the effect on the helix−coil equilibrium quantitatively and to provide a basis for understanding the temperature dependence of the kinetic data, we analyzed the thermal unfolding curves in Figure 2 using a two-state model. According to this model there are only two populations of molecules, one in which there is no helix, and one in which all molecules are completely helical. More realistic models consider the distribution of helical lengths[6] but to establish the approximate magnitude of the equilibrium perturbation caused by the addition of viscogens, the two-state model is sufficient. To obtain the two-state free energy, enthalpy, and entropy changes the temperature dependence of the ellipticity at 220 nm, θ_{220}, was fitted using expressions for the CD of the helix and coil similar to those used by Thompson et al.[6] The ellipticity was assumed to be given by

$$\theta_{220} = f_h(n - n_\alpha)(\theta_\alpha + \theta_{\alpha T}(T - T_0) + \theta_{\alpha W}) + (1 - f_h)(\theta_r + \theta_{rT}(T - T_0) + \theta_{rW}) \quad (1)$$

where f_h is the fraction of helical peptides, n is the length of the peptide, T_0 is 273 K, $\theta_\alpha + \theta_{\alpha T}(T - T_0)$ is the molar ellipticity of the peptide backbone of each residue in an infinite helix at temperature T, and $\theta_{\alpha W}$ is the side-chain contribution of tryptophan in a helix; $\theta_r + \theta_{rT}(T - T_0)$ and θ_{rW} are the corresponding properties for the random coil state. The parameter n_α is an empirical parameter which is introduced to account for the fact that the mean-residue ellipticity is length dependent and is conventionally given a value of about 3 based on the work of Chen et al.[19] The CD parameters obtained by Thompson et al.[6] were used, with the exception of θ_{rW}, which was set to -1.0×10^4 deg cm^2/dm to match the high-temperature data for the sucrose and glucose data sets. The fraction of helical peptides is $f_h = K/K + 1$, where the two state coil ⇌ helix equilibrium constant, K, is assumed to be given by

$$K = \exp\left(-\frac{\Delta H - T\Delta S}{RT}\right) \quad (2)$$

with temperature-independent enthalpy (ΔH) and entropy (ΔS) changes. In fitting the CD data, the values of ΔH and ΔS were varied for each data set. With the exception of the highest concentrations of glycerol and ethylene glycol, the two-state fits are undetectable beneath the data points. The resulting fit parameters are given in Table 1.

TABLE 1: Two-State Thermodynamic Parameters of Helix-Forming Peptide in Mixed Solvents Obtained from Fits to Circular Dichroism Data

dcosolvent (MW)	C (M)	η_{293} (cp)	ΔH (kcal/mol)	ΔS [cal/(mol K)]	K_{293}	T_m (K)	Δk_{max}[a]
none		1.00	−11.6	−39.1	1.25	296	
sucrose	0.63	1.94	−11.4	−38.5	1.33	298	0.97−1.04
(342 D)	0.92	2.85	−10.9	−36.4	1.48	299	0.93−1.10
glucose	1.08	1.76	−11.1	−37.6	1.25	297	1.00−1.00
(180 D)	1.70	2.71	−10.4	−34.8	1.35	298	0.97−1.05
glycerol	2.50	1.84	−10.6	−35.2	1.55	300	0.91−1.14
(92 D)	4.00	2.83	−9.7	−32.1	1.81	304	0.86−1.25
ethylene glycol	4.00	1.86	−9.5	−31.0	1.90	305	0.85−1.29
(62 D)	6.70	2.86	−7.5	−24.0	2.23	313	0.80−1.44

[a] The value of Δk_{max} was calculated as the change in the ratio of the relaxation rate in the cosolvent to the relaxation rate in water, assuming that all of the observed increase in the equilibrium constant results from either an increase in the folding rate (upper limit) or a decrease in the unfolding rate (lower limit).

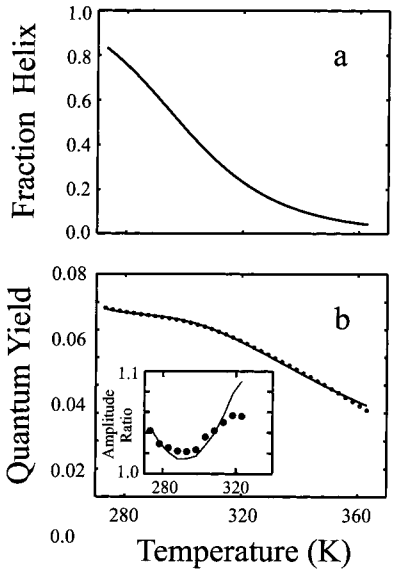

Figure 3. Fluorescence as a function of temperature for helix-forming peptide in 1.7 M glucose. (a) The fraction of helical peptides calculated from the fit to the corresponding data in Figure 2. (b) Fluorescence quantum yield. The points are the data and the continuous curve is the fit obtained using the populations from (a) and eq 3. (Inset) ratio of initial to final amplitudes measured in kinetic experiments in 1.7 M glucose (○) and (—) calculated from the fit in (b).

The results of the two-state analysis in Table 1 quantitatively confirm what is apparent from inspection of the unfolding curves in Figure 2: the sugars glucose and sucrose produce markedly smaller changes in the equilibrium parameters than do the polyols, glycerol and ethylene glycol. In 1.7 M glucose and in 0.91 M sucrose, both of which have viscosities of slightly less than 3 cP at 293 K, the melting temperature (T_m) changes by less than 3 K. The change in T_m for concentrations of glycerol (4.0 M) and ethylene glycol (6.7 M) which produce comparable viscosities was 6 and 16 K, respectively. To establish more precisely how much the relaxation rate would be affected, we calculated the maximum change in the rate that could be produced by the sugars. At ∼3 cP we find that the maximum change in the rate is only ∼5% for glucose and ∼10% for sucrose.

Equilibrium fluorescence curves for this peptide in water have already been reported by Thompson et al.[6] We obtained a set of data at the highest glucose concentration used in our kinetic studies. The results are shown in Figure 3. To fit these data

TABLE 2: Parameters Used in Two-State Fits to Equilibrium Fluorescence Data for Helix-Forming Peptide

k_+/k_s	A_+/k_s	E_+ (kcal/mol)
7.93	1.87×10^4	4.14
k_-/k_s	A_-/k_s	E_-
3.69	1.20×10^4	4.44

with a two-state model, the temperature dependence of the observed fluorescence quantum yield, Φ_{obs}, was described by

$$\Phi_{obs} = f_h\Phi_+ - (1 - f_h)\Phi_- \quad (3)$$

and

$$\Phi_\pm = \frac{k_s}{k_s + k_\pm + A_\pm e^{-E_\pm/RT}} \quad (4)$$

where the subscript (+) denotes the helical state and the subscript (−) the coil state. In eq 4 k_s is the spontaneous emission in the absence of any quenching, $k_\pm$ describes all of the processes assumed to be temperature-independent (intersystem crossing, radiationless decay to the ground state, and proton transfer), and the Arrhenius term corresponds to the quenching rate from electron transfer, which is activated (see discussion by Thomspon et al.[6]). The fluorescence data were fit with the populations (f_h) obtained by optimizing the 6 parameters of eq 4. These values are reported in Table 2.

α-Helix Kinetic Experiments. Figure 4 shows representative kinetic traces from the laser temperature jump experiments on the helical peptide and NATA controls. When the temperature changes, there is an initial sharp decrease in fluorescence for both NATA and the α-helical peptide which results from a decrease in the tryptophan quantum yield. The increased electron-transfer rates reduce the quantum yield of both the coil and helix states of the peptide. The duration of this change is determined by the length of the of the heating laser pulse. Following this rapid decrease, there is a much slower increase in fluorescence intensity from the helical peptide as the population relaxes to a new equilibrium distribution of helix and coil molecules. The fluorescence increases in this relaxation because of the increase in the population of peptides in which the tryptophan is no longer quenched by the protonated histidine. In the NATA controls, there is a small ∼300 ns fluorescence increase following the temperature jump, unrelated to the change in the helix population, which we have modeled as a squared Gaussian (see Methods). The continuous curve through the data for the helical peptide represents the best fit using a single-exponential function. The response functions with the larger amplitudes are the results of fits in which the ∼300 ns fluorescence change was included.

The amplitudes from the exponential fits to the fluorescence kinetics as a function of temperature are compared to the values predicted from the equilibrium curves in the inset to Figure 3b. The reasonably good agreement between the predicted and observed kinetic amplitudes indicates that there are no additional slow phases and is consistent with our treating the data in terms of a two-state system (It also constitutes additional evidence against the suggestion of Clark et al.[20] that helix nucleation occurs with a relaxation time of ∼100 ms).

Three series of temperature-jump experiments were carried out. In the first, the final temperature was held constant at 293 K and the solvent viscosity was varied by adding either glucose or sucrose over the concentration range delimited by the results of the equilibrium experiments. In the second and third, the composition of the solvent was held constant at either 1.7 M

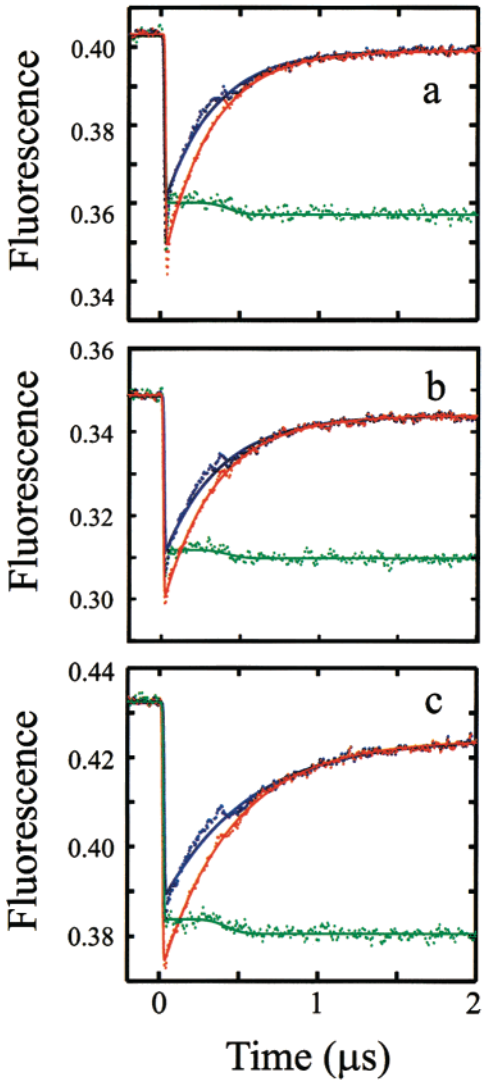

Figure 4. Temperature-jump kinetic data for helix-forming peptide and NATA controls. (a) Data at 293 K, 0.15 M glucose. Temperature jump data on NATA are shown as green dots and temperature jump data for the helix-forming peptide at the same glucose concentration are shown as the blue dots. The fit to the NATA data was obtained using two basis functions: one was a step function with value 1 for negative times and 0 for positive times and the second was zero for negative times and a squared Gaussian (i.e., $\exp[-((t - t_0)/\delta t)^4]$ at positive times. The fitted values of δt and t_0 were 330 and 102 ns and the fitted amplitudes for the two basis functions were 0.0386 and 0.00203. The data for the helix-forming peptide (blue) were fitted using two different procedures. The first fit, shown as the solid blue line, was obtained using two basis functions: the step function described above and a second function which had values of unity at negative times and decayed exponentially as $\exp(-kt)$ at positive times. The fitted value of k is 3.20×10^6 s^{-1} and the amplitudes of the two basis functions are 0.0431 and −0.0393, respectively. The second fit, shown as the red line, was obtained using the same two basis functions plus the squared Gaussian function used to fit the NATA data. The fitted value of k is 2.36×10^6 s^{-1} and the amplitudes of the three basis functions are 0.0562, 0.0520, and 0.0079, respectively. The red data points show the fit to the data after it has been corrected for the fitted amplitude of the squared Gaussian. (b) Data at 293 K, 0.88 M glucose; the fitted rates were 2.83×10^6 s^{-1} with amplitudes of 0.0383 and −0.0335 for the step and exponential components in the simple exponential fit (blue) and 3.03×10^6 s^{-1} with amplitudes of 0.0497 and −0.0449 with the Gaussian pulse included (red). The pulse amplitudes are 0.0026 for the NATA data and 0.0077 for the helix data. (c) Data at 293 K, 1.59 M glucose; the fitted rates were 1.81×10^6 s^{-1} with amplitudes of 0.0439 and −0.0358 for the step and exponential components in the simple exponential fit (blue) and 2.21×10^6 s^{-1} with amplitudes of 0.0595 and −0.0509 with the Gaussian pulse included (red). The pulse amplitudes are 0.0026 in the NATA data and 0.0108 in the helix data. Note that the amplitudes of the Gaussian pulse obtained from the fits of the helix data are 3−4 times larger than those obtained from the NATA data, so it is likely that the fit has overestimated the effect of the pulse. We have therefore used the average value of the rates obtained from the two fits as the reported rate and have used the difference in the two fitted values as the uncertainty in the its determination. At low sugar concentrations this is the total uncertainty but at higher sugar concentrations an additional uncertainty is introduced results by the change in the equilibrium constant (Table 3). The resulting errors are about ±10% at the maximum glucose concentration and about 5% at the maximum sucrose concentration.

glucose (from which the amplitudes were obtained for the inset to Figure 3b) or 0.94 M sucrose, and the temperature was varied. These data, together with the data of Thompson et al.[6] in which kinetics were measured over a similar temperature range in water, provide the database for our analysis of the viscosity and temperature dependence of the kinetics.

Figure 5 shows the dependence of the measured relaxation rates on solvent viscosity at constant temperature. The data fall on a straight line in this log−log plot with slopes of -0.59 ± 0.06 for glucose and -0.53 ± 0.06 for sucrose. The large uncertainties on these values reflect the variations which result from the use of the two different fitting procedures. For either procedure alone, the errors are much smaller (±0.02), suggesting that the difference in slopes is significant.

The uncertainty resulting from the changes in equilibrium constant (Table 1) are comparable, so that the total uncertainty in these slopes, including both random and systematic errors is about ±0.1.

Figure 6 shows the observed relaxation rates as a function of temperature. The temperature dependence of the solvent viscosities is also shown (inset). The observation of parallel curves for both the relaxation rates and viscosity indicates that the viscogenic agents are not perturbing either the equilibrium constant or the activation energy. This was demonstrated quantitatively by the following analysis.

The lack of a simple inverse first power viscosity dependence prompted us to analyze the data at various temperatures with three different functional forms. For a two state system with folding and unfolding rate constants, k_f and k_u, the observed relaxation rate k_{obs} is given by

$$k_{obs} = k_f + k_u = F(\eta) \exp\left(-\frac{E_0}{RT}\right)\left(1 + \frac{1}{K}\right) \qquad K \equiv k_f/k_u \quad (5)$$

where $F(\eta)$ is the reduced rate ($\equiv k_f \exp(+E_0/RT)$ and is a function of solvent viscosity. Equation 5 shows that there are three contributions to the temperature dependence of the observed relaxation rate, one from the change in solvent viscosity with temperature, a second from the activation energy, and a third from the temperature dependence of the equilibrium constant. If we have the correct functional form for the viscosity, then the data at all temperatures and viscosities will be described by this equation, provided of course that the barrier height E_0, in addition to the equilibrium constant K, is unaffected by the

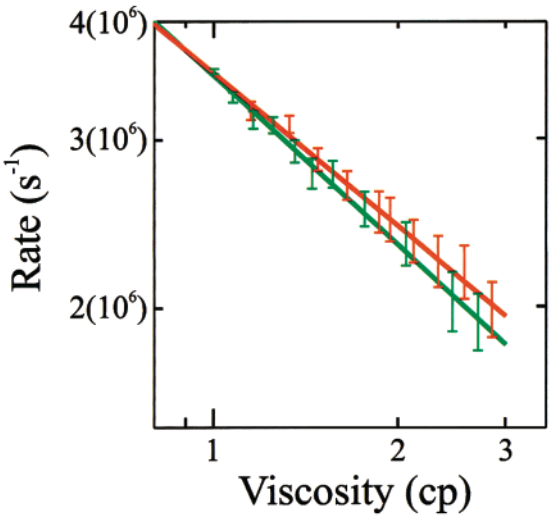

Figure 5. Dependence of observed relaxation rate for helix-forming peptide on viscosity at 293 K. (a) The logarithm of the relaxation rate as a function of the logarithm of the viscosity. The rates obtained from both fits described in Figure 4 are plotted as the horizontal bars for glucose (green) and sucrose (red). The straight line is a fit of eq 6 to the means of the two fitted values. The fitted values of the parameters are $\alpha = 0.53$, $A = 3.5 \times 10^6$ for sucrose and $\alpha = 0.59$, $A = 3.5 \times 10^6$ for glucose. To estimate the uncertainty in the fitted values, we fitted the rates obtained by each fitting procedure independently. For sucrose the resulting slopes are $\alpha = 0.59$ and $\alpha = 0.48$, while for the lower molecular weight glucose the slopes are $\alpha = 0.65$ and $\alpha = 0.52$. The uncertainty in the slopes obtained from either fitting procedure is ± 0.02

viscogenic agents. We tried three functional forms for $F(\eta)$: the empirical power-law function

$$F(\eta) = A\eta^{-\alpha} \tag{6}$$

the hydrodynamic form of Kramers equation at intermediate friction[13]

$$F(\eta) = \frac{B\eta}{C}\left\{\left[1 + \left(\frac{C}{\eta}\right)^2\right]^{1/2} - 1\right\} \tag{7}$$

and the modification of the high-friction Kramers equation (eq 6 with $\alpha = 1$) by Ansari et al.[21]

$$F(\eta) = \frac{D}{\sigma + \eta} \tag{8}$$

which includes a contribution from internal friction, σ.

To carry out the fit, all of the data were assembled in a file which contained the experimental temperatures, viscosities, relaxation rates, and equilibrium constants. The parameters were then varied to optimally reproduce the experimental relaxation rates, calculated using eq 5 with either eqs 6, 7, or 8 for $F(\eta)$. The parameters from these fits are summarized in Table 3. As can be seen from the curves through the data in Figure 6, the errors in the fit using the three different functional forms for the viscosity are similar. However, the final sum of squares is significantly larger using Kramers' eq 7, than for either of the other two functional forms for the viscosity dependence. This can be seen in plots of the reduced folding rate (at all temperatures) (Figure 7). The extent to which the reduced rates at all temperatures and viscosities collapse onto a single curve is a measure of the accuracy of the functional form of $F(\eta)$ (assuming a constant activation energy). It is interesting to note that the value of $\alpha = 0.64 \pm 0.07$ obtained using eq 6 is close to the average value obtained from the isothermal data (Figure 5).

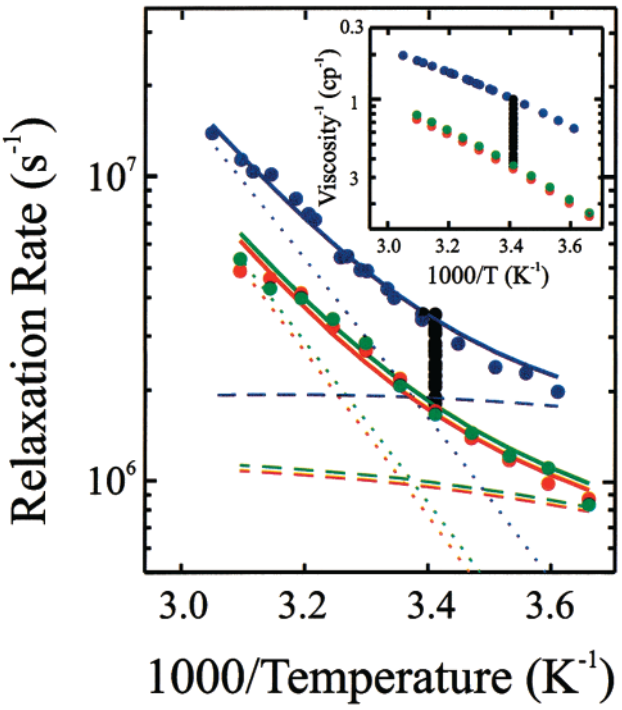

Figure 6. Temperature dependence of the relaxation rates for helix-forming peptide. Measured relaxation rates for water (blue) sucrose (red) and glucose (green) and the isothermal data in Figure 5 (black) plotted as filled circles. The continuous lines are the fits to the two state kinetic model using eq 6 to describe the viscosity dependence of the folding rates. The dashed lines are the calculated folding rates and the dotted lines are the calculated unfolding rates. In the inset, the reciprocal of the solution viscosity is plotted as a function of $1/T$ for the solution conditions used in these experiments. To permit direct comparison of slopes in the two plots, the aspect ratios are identical.

***β*-Hairpin Equilibrium Experiments.** Demonstrating the effects of viscogenic agents on folding/unfolding equilibrium of the β-hairpin from protein GB1 is more problematic. Circular dichroism is not nearly the sensitive and accurate measure of β-structure formation that it is for the α-helix. Figure 8 shows that at concentrations of glucose and sucrose that produce viscosities up to ~1.5 and ~2 cP, respectively, the circular dichroism spectrum at 273 K is unaffected, as is the thermal unfolding curve monitored by the ellipticity at the minimum at 201 nm. At higher concentrations (viscosities) of these sugars there are clear deviations (data not shown). To analyze the equilibrium effects quantitatively, we used the thermal unfolding curves determined by fluorescence, as was done by Muñoz et al.[8] The quantum yield as a function of temperature for this peptide and for the reference peptide GEWTY are shown in Figure 9. To fit these data, the fluorescence of the control peptides in each cosolvent was first fitted using eqs 3 and 4. The results of the study on the GB1 peptide by Muñoz et al.,[8] and the more recent study of Honda et al.[22] were used to weakly constrain the enthalpy change for folding and the equilibrium constant at 273 K. It was then assumed that the fluorescence of the unfolded form of the peptide could be accurately modeled as that of the reference peptide in the same solvent and that only the parameters k_+ and A_+ changed when the hairpin folded (the value of E in each solvent was assumed to be identical to that for the reference peptide). The rationale for this approach was that the access to solvent in the folded hairpin should reduce the quenching efficiencies relative to that for the reference peptide. The constrained folding equilibrium parameters and the fluorescence parameters for the folded hairpin were then optimized to reproduce the measured fluo-

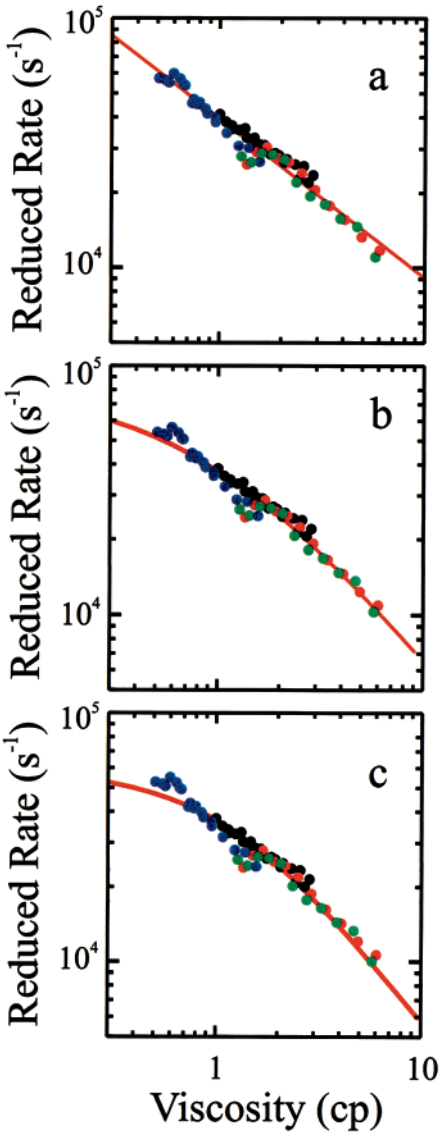

Figure 7. Reduced folding rates for helix-forming peptide. The reduced folding rates, defined as $k_f \exp(+E_0/RT)$, were obtained from fits to all of the data using (a) eq 6, (b) eq 8 or (c) eq 7 to describe the viscosity dependence of the folding rate.

TABLE 3: Parameters from Fit to Kinetic Data Using Different Viscosity Functions for Helix-Forming Peptide

empirical eq 6	A (s^{-1} cP^{α})	α	E_0 (kcal/mol)	final sum-of-squares
	3.97×10^4	0.64 ± 0.07	−2.24	0.400
Kramers eq 7	B (s^{-1})	C (cP)		
	6.17×10^4	1.88	−2.29	0.583
internal friction eq 8	D (s^{-1})	σ (cP)		
	7.12×10^4	0.88 ± 0.10	−2.28	0.449

rescence curves for the folding hairpin. The resulting parameters are shown in Table 4. Also shown in Table 4 are the results obtained when the constraints on the equilibrium parameters are removed. The net effect is to reduce the value of ΔH and to slightly decrease T_m. In both fits, the quenching rates are 30−60% smaller than those for the control peptide so the fluorescence of the folded peptide is less temperature-dependent than that of the unfolded (reference) peptide. In addition, the calculated quantum yield of the folded β-hairpin peptide is less solvent-dependent than that of the reference peptide (Figure 9). Since a significant fraction of tryptophan is buried in the folded hairpin, changes in solvent composition would be anticipated to have a smaller effect on the quantum yield, as observed.

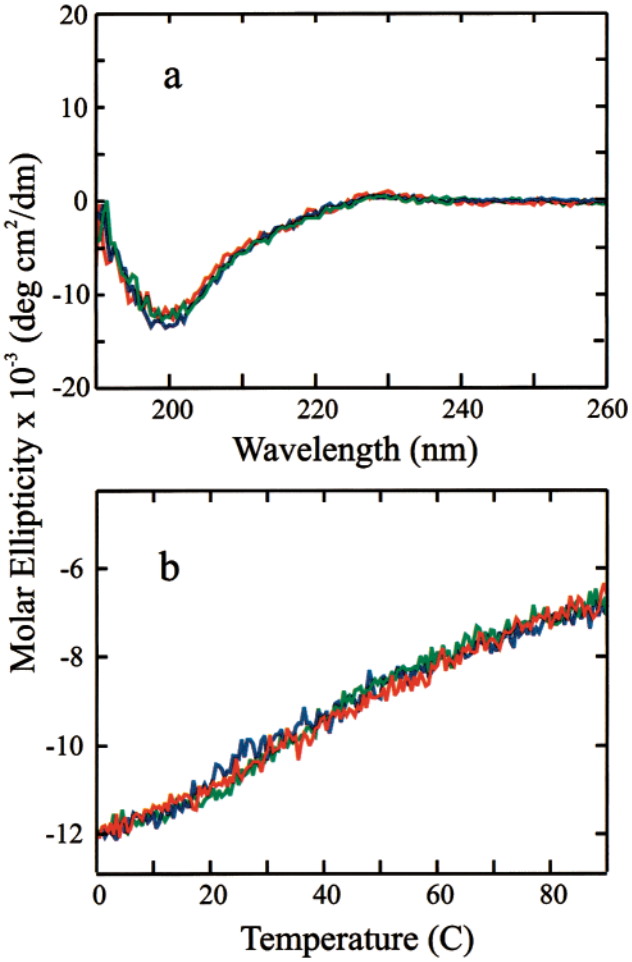

Figure 8. Circular dichroism of the hairpin forming peptide. (a) Circular dichroism spectra at 273 K measured in water (blue), 1.33 M glucose (red), and 0.37 M sucrose (green). (b) Ellipticity at 201 nm as a function of temperature in water (blue), 1.3 M glucose (green), and 0.37 M sucrose (red).

***β*-Hairpin Kinetic Experiments**. Figure 10 shows representative kinetic traces. There is a rapid decrease in fluorescence, coincident with the heating laser pulse, followed by a much slower single-exponential phase corresponding to a decrease in the hairpin population. In contrast to the helix, the fluorescence increases because water is a more efficient quencher of tryptophan fluorescence than the valine and phenylalanine that it contacts in the hydrophobic cluster (Figure 1).

As for the helical peptide, a series of temperature-jump experiments were carried out. In the first, the temperature was held constant at 293 K and the solvent viscosity was varied by addition of either glucose or sucrose over the range delimited by the results of the equilibrium experiments (Figure 11). In the others, the solvent composition was held constant − either aqueous buffer, 1.33 M glucose or 0.37 M sucrose, and the temperature was varied (Figure 12). In contrast to the helix, both the isothermal data and the more extensive analysis using eqs 5 and 6 yielded viscosity exponents close to unity. In the isothermal plots (Figure 10) the slopes for glucose and sucrose are -0.92 ± 0.03 and -0.95 ± 0.03, respectively. Analysis using eqs 5 and 6 show that a good fit is obtained with $\alpha = 1.07 \pm 0.25$ (Figure 12), as is evident from the collapse of all of the data onto a single curve (Figure 13). Recognizing that the equilibrium analysis is less certain than that carried out for the helix-forming peptide, we cannot conclude that the rate of hairpin formation varies significantly from a perfect inverse first power viscosity dependence.

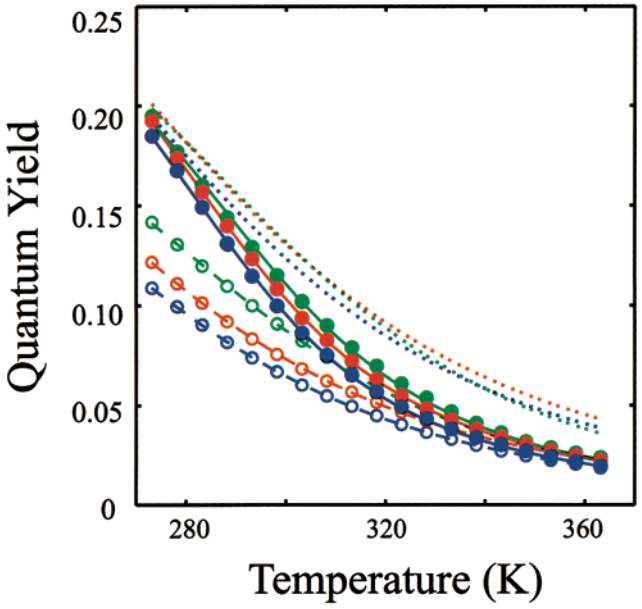

Figure 9. Dependence of fluorescence quantum yield on temperature for hairpin-forming peptide (filled circles) and the reference peptide GWETY (open circles). Data are shown in water (blue), 0.37 M sucrose (red) and 1.33 M glucose (green). The lines through the lower data are fits to the reference peptide data using eq 3, with the parameter values given in Table 2. The lines through the upper data points are the fits to the two-state populations of hairpin and unfolded peptides using the fluorescence of the reference peptide to describe the unfolded hairpin and the fitted temperature dependence of the fluorescence of the folded peptide in each solvent which is shown as the upper dashed lines.

TABLE 4: Two-State Thermodynamic Parameters of Hairpin-Forming Peptide in Mixed Solvents Obtained from Fits to Fluorescence Data

	Thermodynamic Parameters		
	ΔH (kcal/mol)	ΔS [cal/(mol K)]	T_m (K)
constrained	−11.7	−38.7	301
free	−10.0	−33.3	300
	Fluorescence Parameters Control Peptide		
	k_-/k_s	A_-/k_s	$E_\pm$ (kcal/mol)[a]
water	3.38	4.79	5.07
0.37 M sucrose	2.92	4.29	4.94
1.33 M glucose	3.64	2.45	6.18
	Folded Hairpin Peptide		
	k_+/k_s	A_+/k_s	
	Constrained		
water	1.89	3.07	5.07
0.37 M sucrose	2.07	2.02	4.94
1.33 M glucose	1.78	1.45	6.18
	Unconstrained		
water	1.72	2.80	5.07
0.37 M sucrose	2.00	2.03	4.94
1.33 M glucose	1.82	1.45	6.18

[a] Model assumes the same activation energy for folded and unfolded species.

Discussion

One problem often plagues kinetic studies on the effect of viscosity. Changes in the solvent can also alter the energy surface, making it difficult to disentangle the thermodynamical from the dynamical effects. To obtain the purely dynamical effect it is therefore necessary to demonstrate that the energy surface remains unchanged. In this study we have used both equilibrium and kinetic criteria to show that our results are not

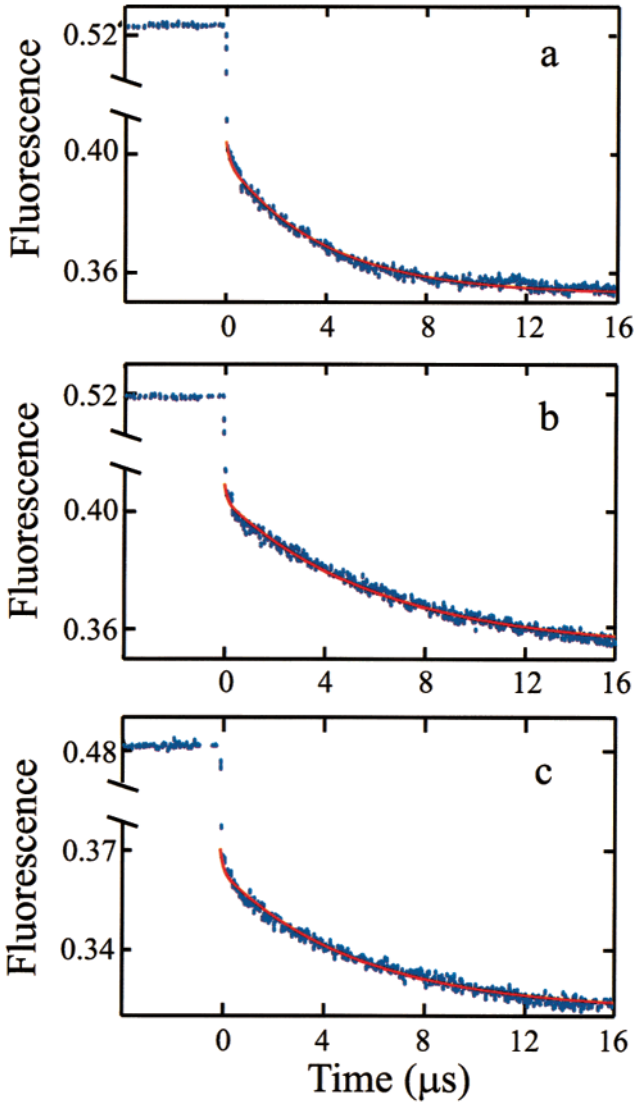

Figure 10. Temperature jump kinetic data (blue) and exponential fits for hairpin-forming peptide at 293 K. (a) water; fitted relaxation time 3.0 μs, (b) 1.33 M glucose; $\eta = 2.1$ cP, fitted relaxation time 6.0 μs, (c) 0.37 M sucrose, $\eta = 1.5$ cP, fitted relaxation time is 4.3 μs.

affected by changes in the energy surface. First, we analyzed the effect of the viscogenic agents on the thermal unfolding curves determined from circular dichroism and fluorescence measurements. This analysis assumed a two-state model for each peptide. In the case of the hairpin-forming peptide evidence for two-state behavior comes from previous studies showing the same equilibrium behavior and identical, single-exponential relaxation rates with two different optical probes.[8] More recently two state behavior has been confirmed in a detailed NMR study of chemical shifts of 14 of the16 residues of this peptide and the finding of the same values for the calorimetric and two-state Van't Hoff enthalpies.[22] Finally, statistical mechanical modeling of the equilibrium and kinetic data also suggest that the hairpin should behave as a near-perfect two-state system.[8,9] Much more is known about helix formation, and it is generally thought to be a more complex system because of the temperature dependence of the distribution of helical segment lengths.[23] Two-state fits to the circular dichroism curves show barely perceptible deviations from the experimental data (Figure 2). In addition, the kinetic progress curves for this peptide are well-described with single exponential functions (Figure 4), so for the present purpose a two-state model is also sufficient to describe the

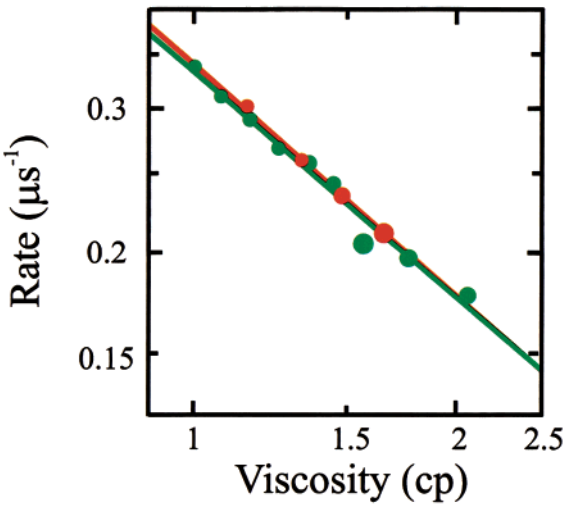

Figure 11. Dependence of the observed relaxation rate for the hairpin peptide on viscosity at 293 K. (a) The logarithm of the relaxation rate is plotted as a function of the logarithm of the viscosity. for glucose (green) and sucrose (red). The slopes of the best straight line fits to the glucose and sucrose data are −0.92 ± 0.03 and −0.95 ± 0.03, respectively.

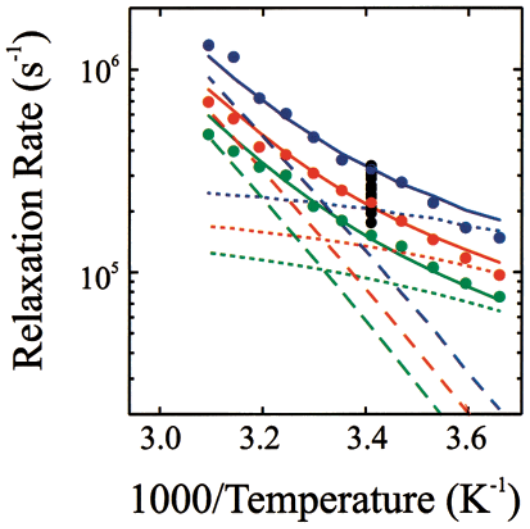

Figure 12. Temperature dependence of the relaxation rates for the hairpin-forming peptide. (a) Measured relaxation rates for water (blue) sucrose (red) and glucose (green) and the isothermal data in Figure 5 (black) plotted as circles. The solid lines are the fits to the two state kinetic model using eqs 5 and 6 to describe the observed rates with $A = 1.3 \times 10^3\ s^{-1}\ cP^a$, $a = 1.07$, and $E_0 = -2.9$ kcal/mol. The dashed lines are the calculated folding rates and the dotted lines are the calculated unfolding rates.

kinetics. The increased cooperativity of this helix is presumably due to the tryptophan-histidine and histidine-arginine interactions.[6] The net result of the analysis is that there is only a very small effect of the viscogenic agents glucose and sucrose on the folding/unfolding equilibrium for both the α-helix and the β-hairpin up to concentrations producing viscosities of ∼3 and ∼2 cP, respectively, at 293 K ($\eta(H_2O) = 1$ cP).

Kinetic measurements at constant temperature in this range of concentrations show that there is a large difference between the viscosity dependence of the relaxation rate for the α-helix and β-hairpin forming peptides. This can be readily seen in logarithmic plots of the rate versus viscosity, which are linear and yield a slope close to −1 for the hairpin (Figure 11) and a slope of only about −0.6 for the-helix forming peptide (0.59 ± 0.1 for glucose and 0.53 ± 0.1 for sucrose; these uncertainties

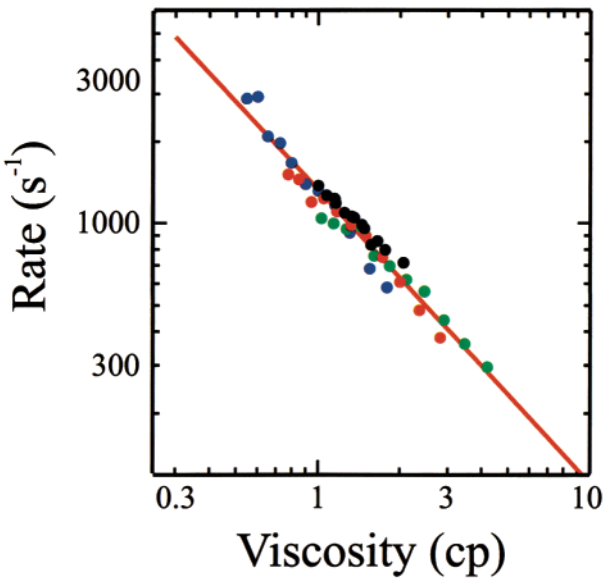

Figure 13. Reduced folding rates for hairpin-forming peptide. The data were fitted using eq 6 to describe the viscosity dependence.

include the effect on the relaxation rate produced by the small changes in equilibrium constants, i.e., Δk_{max} in Table 1) (Figure 5). While the very small effect on the thermal unfolding curves indicates that the wells of the energy surface are essentially unperturbed over the range of sugar concentrations in these experiments, it does not guarantee that the barriers are unaffected. To determine whether the addition of sugars affects the activation energies and to expand the viscosity range of the kinetic measurements, we investigated the temperature dependence of the relaxation rates at a fixed sugar concentration. The data at all temperatures and viscosities were then fit simultaneously to a two-state model (eq 5) using the viscosity dependence of eq 6. For the β-hairpin-forming peptide the data could be well-fit assuming that the rate again varies very nearly as the inverse first power of the viscosity ($\alpha = 1.07 \pm 0.25$ in eq 6). For the α-helix forming peptide a fractional viscosity dependence was observed with $\alpha = 0.64 \pm 0.07$, close to the average found for the individual sugars in the isothermal data. The results on the viscosity dependence at all temperatures are summarized in log−log plots of the reduced folding rate ($\equiv k_f \exp(+E_0/RT)$) versus viscosity (Figures 7 and 13). The observation that the reduced folding rates collapse onto a single curve is a measure of the accuracy of the fit. Assuming a power-law for the viscosity dependence (eq 6), as observed for the isothermal data (Figures 5 and 11), the finding of a satisfactory fit using the two state model of eq 5 demonstrates that the intrinsic activation energies are not significantly altered over the entire range of solvent compositions and temperatures studied.[24] Thus, both the wells and barriers appear to remain unaffected by increasing the viscosity with glucose and sucrose. Their effect on the kinetics therefore arises entirely from the dynamical effect of the change in solvent viscosity.

Our problem is to explain why the viscosity dependence for the rates of α-helix and β-hairpin formation is so different. To discuss this question, it is instructive to first briefly consider the origins of Kramers theory.[13,25] The central equation for describing the dynamics of a unimolecular process in solution is the stochastic Langevin equation in one dimension:

$$\mu\ddot{x} = -\partial U(x)/\partial x - \zeta\dot{x} + R(t) \qquad (9)$$

In this highly idealized treatment the change in the molecular

structure is represented as Brownian motion of a single effective particle of reduced mass μ in the one-dimensional potential, $U(x)$. Collisions of the solvent with the particle influence its motion in two ways. They cause friction, which is an opposing force proportional to the velocity, $\dot{x}$, characterized by the coefficient ζ. Collisions also produce a "random" force, $R(t)$. There is an exact relation between these energizing and de-energizing terms (the fluctuation dissipation theorem). Kramers showed that the rate constant for a particle escaping from a parabolic well A over an inverted parabolic barrier B of height E_0 is given by

$$k = \frac{\omega_A}{2\pi}\left\{\left[1 + \left(\frac{\gamma}{2\omega_B}\right)^2\right]^{1/2} - \frac{\gamma}{2\omega_B}\right\} \exp\left(-\frac{E_0}{k_B T}\right) \quad (10)$$

where the damping rate $\gamma = \zeta/\mu$, and the frequencies ω_A and ω_B measure the curvature of the well and barrier top, respectively. If the friction is sufficiently high such that $\gamma \gg \omega_B$, then the Kramers rate simply becomes

$$k = \frac{\omega_A \omega_B}{2\pi\gamma} \exp\left(-\frac{E_0}{k_B T}\right) \quad (11)$$

which is often called the Smoluchowski limit because it can be derived from Smoluchowski's diffusion equation. In eqs 10 and 11, the friction is generally assumed to come entirely from the solvent. However, friction arising from the exchange of energy occurring in collisions between solute atoms may also contribute. Ansari et al.[21] suggested a modification of eq 11 to account for the effect of this so-called internal friction. They assumed that the total damping rate is a linear combination of the internal (γ_i) and the solvent (γ_s) contributions, i.e.

$$k = \frac{\omega_A \omega_B}{2\pi(q\gamma_i + (1-q)\gamma_s)} \exp\left(-\frac{E_0}{k_B T}\right) \quad (12)$$

where q is the fractional contribution from the internal friction (which itself could depend on solvent viscosity[26]). Equations 10−12 predict that increasing the friction will slow the rate, while increasing either the well or barrier frequency will increase the rate.[27]

The Langevin equation (eq 9) assumes that the collisions with the solvent are instantaneous and that the solvent relaxation is fast relative to the motion across the barrier top. To compare the predictions of eqs 10−12 with experiment, the damping rate γ is replaced by the macroscopic shear viscosity η using Stokes law ($\zeta = 6\pi r\eta$) for diffusion of a particle of radius r in a continuous medium. The exponential prefactors in eqs 10, 11, and 12 then become eqs 7, 6 (with $\alpha = 1$), and 8 respectively, where $B = \omega_A/2\pi$ and $C = \mu\omega_B/3\pi\rho r$.

From the preceding discussion it would appear that there are two possible origins for a fractional viscosity dependence − one is a breakdown of Kramers theory and the second is a deviation from Stokes law. We first consider the failure of Stokes law. Investigations of the rates of photoisomerization reactions have frequently shown a viscosity dependence characterized by a power law with $0 < \alpha < 1$, which cannot be fit by the Kramers intermediate friction equation 10.[10,11] To distinguish between a breakdown of Kramers theory and failure of Stokes law, Velsko et al.[10] determined the viscosity dependence of the rotational correlation time in their isomerization study of a cyanine dye (DODCI). They reasoned that the friction opposing the barrier crossing would be more similar to the friction experienced by the rotating molecule than to the friction determined from the macroscopic shear viscosity (i.e., from Stokes law). However, they found that the rotational correlation time was proportional to η, suggesting that failure of Stokes law was not the origin of the fractional viscosity dependence of the rate. On the other hand Lee et al.[28] found that for stilbenes the rotational correlation time is not proportional to viscosity when the solvent molecules become larger than the solute, and so could account for the apparent deviation from the Kramers eq 10 as arising from the failure of Stokes law.

In our experiments there is an additional complication because cosolvents were used to increase the viscosity. Studies by Barshtein et al.[29] on the self-diffusion of water in aqueous solutions of various viscogenic cosolvents showed large deviations from Stokes−Einstein ($D = k_B T/\zeta$) behavior, i.e., $D \propto \eta^{-1}$. They found $D \propto \eta^{-\beta}$, where the value of β decreases markedly with increasing molecular weight of the cosolvent, and can be approximated by $\beta \propto (M_0/M)^{1/3}$, where M_0 is the molecular weight of water and M is the cosolvent molecular weight. This has often been called the effect of microviscosity—rotational or translational motion of a small molecule in an aqueous solution made viscous by the addition of much larger molecules encounters less friction than that measured by the macroscopic shear viscosity. For glucose Barshtein et al.[29] found $\beta \approx 0.4$, while for sucrose $\beta \approx 0.3$. We have found a slightly smaller viscosity exponent for sucrose (0.53) compared to glucose (0.59) for the helix (Figure 5). Since sucrose is about twice the size of glucose, this result may suggest a small contribution from this microviscosity effect. However, the very similar exponents for glucose and sucrose together with the near unity viscosity exponent for the hairpin suggest that failure of Stokes law due to this microviscosity effect is not the origin of the fractional viscosity dependence for the helix.

The question then becomes whether the fractional viscosity dependence can be accounted for by Kramers intermediate friction model (eqs 7 and 10) or by the Kramers high friction model which includes the effect of internal friction (eqs 8 and 12). Both the results of our experiments and theory suggest that dynamics in the intermediate friction regime is an unlikely explanation for the fractional viscosity dependence. In fitting our experimental data at all viscosities and temperatures, we find a significantly worse fit using the Kramers intermediate friction model (eq 7), than with either the power law (eq 6) or internal friction (eq 8) models (Table 3, Figure 7). This result is consistent with Langevin simulations of simplified representations of α-helix forming and β-hairpin forming peptides by Klimov and Thirumalai.[30] They found that at frictions corresponding to water the Kramers high friction limit had already been reached; i.e., the rates of both hairpin and helix formation are proportional to the inverse first power of the friction coefficient used in the simulations. In this friction range Loncharich et al.[31] also found an inverse first-power dependence in their Langevin simulations of isomerization of an all atom representation for a peptide (*N*-acetylalanyl-*N*-methylamide).

Although the internal friction equation can fit the data nearly as well as the power law (Table 3, Figure 7), there are several reasons why it is probably not the correct explanation. First, Ansari et al.[21] used this equation to explain the viscosity dependence for the conformational change of a native compact protein in which a large fraction of the atoms do not collide with solvent atoms (they found a viscosity-independent rate at the viscosities of water and an inverse first power dependence above ∼15 cP, corresponding to $\sigma \approx 4$ in eq 8). If internal friction made a significant contribution in peptide folding we would expect a much smaller value for σ, since the solvent

exposure is much greater. Second, there is no compelling reason to expect a larger contribution from internal friction for helix formation than for hairpin formation. Finally, Loncharich et al.[31] did observe internal frictional effects in their Langevin simulations, but at solvent frictions corresponding to viscosities more than ~10-fold smaller than that of water at room temperature.

We are therefore left with explaining the fractional viscosity dependence as resulting from a breakdown of the one-dimensional Kramers theory. Previous studies on chemical systems have reached a similar conclusion and so provide a guide for further interpretation. Both Velsko et al.[10] and Rothenberg et al.[11] suggested that the extension of Kramers theory by Grote and Hynes[14] to include the frequency-dependent friction in the Langevin equation (eq 9) could explain their finding of a fractional viscosity dependence. This extension relaxes the Brownian motion assumption of Kramers that collisions are effectively instantaneous and therefore that solvent relaxation is much faster than the barrier crossing event. Since slow solvent motions do not contribute to the barrier-crossing friction, the friction is lower than that obtained from the macroscopic (zero-frequency) shear viscosity of Stokes law. In the Grote−Hynes theory the friction coefficient of eq 9 is no longer proportional to the macroscopic shear viscosity, but depends on the frequency at the barrier top, with lower friction for sharper barriers. Calculations of the frequency dependent friction coefficient are difficult, but indicate that over the range of viscosities studied experimentally a power-law dependence is obtained using the Grote−Hynes formulas.[32]

A possible key to explaining the difference in viscosity exponents for the α-helix and β-hairpin in our experiments is the interesting suggestion of Velsko et al.[10] that the smaller value for the viscosity exponent α for the ground-state isomerization ($\alpha = 0.26$) compared to the excited-state photoisomerization ($\alpha = 0.43$) results from a much higher energy barrier in the latter (E_0(ground state) ≈ 14 cal/mol; E_0(excited state) = 3 kcal/mol) (see also Vauthey[33]). They argued that smaller barriers are generally flatter, and that a lower barrier frequency decreases the separation in time scales between the molecule and solvent motions. This would result in a more diffusive barrier crossing, and therefore a higher viscosity dependence. A similar argument has been presented by Zhu and Ediger,[12] who used nuclear magnetic resonance measurements to study the viscosity dependence of the reorientational correlation time of the backbone C−H vector in various homopolymers. They found a fractional viscosity dependence with an exponent that increased monotonically from 0.3 to 1.0 with increasing molecular weight of the polymer side chain (interestingly, their plot of exponent versus side chain molecular weight predicts an exponent of 0.6 for the average side chain molecular weight of the helix-forming peptide of our study). They suggested that the larger molecular weight of the side chain would produce a lower barrier frequency, both because of its size and a larger moment of inertia.

The explanation proposed by Velsko et al.[10] for the difference in viscosity exponents might also explain the difference in the exponents for the hairpin and helix. Using a simple statistical mechanical model in which the elementary step in forming secondary structure is the rotation of a pair of backbone dihedral (ϕ,ψ) angles, the activation energy for an individual step was found to be much larger for the helix than the hairpin. Assuming a viscosity exponent of unity for every step, Muñoz et al.[9] found the best fit to the temperature dependence of the hairpin relaxation rates yielded an activation energy of zero. In contrast, Thompson et al.[6] found an intrinsic activation energy of 4.5−5.7 kcal/mol, after correcting the temperature dependence with a viscosity exponent of 0.7 for each step of helix formation. Following the logic of Velsko et al.[10] the zero activation energy for the elementary kinetic steps of forming a β-hairpin suggests a barrier which is flatter than for the α-helix and therefore a more diffusive barrier crossing. For α-helix formation the sharper barrier, associated with the higher activation energy, would result in faster barrier crossing that might require a time-dependent friction coefficient.

In summary, we have measured the effect of viscosity on the relaxation rates associated with the formation of two different types of protein secondary structure − an α-helix and a β-hairpin. These measurements were made at concentrations of sugars that increase the viscosity, but have little or no effect on either the equilibrium constants or activation energies. The somewhat surprising result is that there is a marked difference between the viscosity dependence of the kinetics of α-helix and β-hairpin formation. There appears to be a plausible connection between the viscosity exponents and the energy barriers for the elementary kinetic steps of a simple model. These findings suggest that it would be important to carry out additional experimental studies on peptides of varying composition to determine whether the difference in the viscosity dependence for the different types of secondary structure is a general result.

Acknowledgment. We thank Robert Zwanzig, Attila Szabo, Peggy Thompson, and Victor Muñoz for helpful discussions.

References and Notes

(1) Onuchic, J.; Luthey-Schulten, Z.; Wolynes, P. G. *Annu. Rev. Phys. Chem.* **1997**, *48*, 545−600. Shakhnovich, E. I. 1997. *Curr. Opin. Struct. Biol.* **1997**, *7*, 29−40. Pande, V. S.; Grosberg, A. Y.; Tanaka, T.; Rokhsar, D. S. *Curr. Opin. Struct. Biol.* **1998**, *8*, 68−79. Dobson, C. M.; Sali, A.; Karplus, M. *Angew. Chem., Int. Edit.* **1998**, *37*, 868−93. Chan, H. S.; Dill, K. A. *Proteins* **1998**, *30*, 2−33. Thirumalai, D.; Klimov, D. *Curr. Opin. Struct. Biol.***1999**, *9*, 197−207.

(2) Callender, R. H.; Dyer, R. B.; Gilmanshin, R.; Woodruff, W. H. *Annu. Rev. Phys. Chem.* **1998**, *49*, 173−202. Gruebele, M. *Annu. Rev. Phys. Chem.* **1999**, *50*, 485−516. Eaton, W. A.; Muñoz, V.; Hagen, S. J.; Jas, G. S.; Lapidus, L. J.; Henry, E. R.; Hofrichter, J. *Annu. Rev. Biophys. Biomol. Struct.* **2000**, *29*, 327−359.

(3) Hofrichter, J.; Thompson, P. A. In *Protein Stability and Folding*, 2nd ed.; Murphy, K. P., Ed.; Humana Press: Totowa, NJ (in press).

(4) Williams, K.; Causgrove, T. P.; Gilmanshin, R.; Fang, K. S.; Callender, R. H.; Woodruff, W. H.; Dyer, R. B. *Biochemistry* **1996**, *35*, 691−697.

(5) Thompson, P. A.; Eaton, W. A.; Hofrichter, J. *Biochemistry* **1997**, *36*, 9200−9210.

(6) Thompson, P. A.; Muñoz, V.; Jas, G. S.; Henry, E. R.; Eaton, W. A.; Hofrichter, J. *J. Phys. Chem. B* **2000,** *104*, 378−389.

(7) Lednev, I. K.; Karnoup, A. S.; Sparrow, M. C.; Asher, S. A. *J. Am. Chem. Soc.* **1999**, *121*, 8074−8086.

(8) Muñoz, V.; Thompson, P. A.; Hofrichter, J.; Eaton, W. A. *Nature* **1997**, *390*, 196−199.

(9) Muñoz, V.; Henry, E. R.; Hofrichter, J.; Eaton, W. A. *Proc. Natl. Acad. Sci. U.S.A.* **1998**, *95*, 5872−5879.

(10) Velsko, S. P.; Waldeck, D. H.; Fleming, G. R.; *J. Chem. Phys.* **1983**, *78*, 249−258.

(11) Rothenberger, G.; Negus, D. K.; Hochstrasser, R. M. *J. Chem. Phys.* **1983**, *79*, 5360−5367.

(12) Zhu, W.; Ediger, M. D. *Macromolecules* **1997**, *30*, 1205−1210.

(13) Kramers, H. A. *Physica* **1940**, *7*, 284−304.

(14) Grote, R. F.; Hynes, J. T. *J. Chem. Phys.* **1980**, *73*, 2715−2732.

(15) Daura, X.; Jaun, B.; Seebach, D., van Gunsteren, W. F.; Mark, A. E. *J. Mol. Biol.* **1998**, *280*, 925−932. Duan, Y.; Kollman, P. A. *Science* **1998**, *282*, 740−744.

(16) Gronenborn, A. M.; Filpula, D. R.; Essig, N. Z.; Achari, A.; Whitlow, M.; Wingfield, P. T. G. M.; Clore, G. M. *Science* **1991** 253, 657−661.

(17) Gill, S. C.; von Hippel, P. H. *Anal. Biochem.* **1989**, *73*, 319−326.

(18) Chen, R. F. *Anal. Lett.* **1967**, *1*, 35−42.

(19) Chen, T.-H.; Yang, J. T.; Chau, K. H. *Biochemistry* **1974**, *13*, 3350−3359.

(20) Clarke D. T.; Doig A. J.; Stapley B. J.; et al. *Proc. Natl. Acad. Sci. U.S.A.* **1999** 96, 7232−7237.

(21) Ansari, A.; Jones, C. M.; Henry, E. R.; Hofrichter, J, Eaton, W. A. *Science* **1992**, *256*, 1796−1798.

(22) Honda, S.; Kobayashi, N.; Munekata, E.; et al. *J. Mol. Biol*. **2000**, 295, 269−278.

(23) Chakrabarty, A.; Baldwin, R. L. *Adv. Prot. Chem.* **1995**, *46*, 141−176. Muñoz, V.; Serrano, L. *J. Mol. Biol.* **1995**, *245*, 275−296.

(24) Using these exponents to correct the observed rates for the temperature dependence of the viscosity of water ($E_\eta = 4$ kcal/mol in the range 0−50 °C), we obtain apparent activation energies for folding the helix and hairpin, which are both negative ($E_{\text{helix}} = -2.2$ kcal/mol; $E_{\text{hairpin}} = -2.9$ kcal/mol). Muñoz et al. have already pointed out that in their model the hairpin transition state contains backbone-backbone hydrogen bonds that place it at a lower energy than the unfolded state, providing a ready explanation of the apparent negative activation energy obtained from the two-state analysis. At least part of the negative activation energy obtained from a two-state analysis of helix formation may have a similar explanation, but this issue requires further exploration.

(25) Hynes, J. T. In *Theory of Chemical Reaction Dynamics*; Baer, M., Ed; CRC Press: Boca Raton, FL 1985,5; p 171. Berne, B.; Borkovec, M.; Straub, J. E. *J. Phys. Chem.* **1988**, *92*, 3711−3725. Hänggi, P.; Talkner, P.; Borkovec, M. *Rev. Mod. Phys*. **1990**, *62*, 251−341.

(26) Vitkup, D.; Ringe, D.; Petsko, G. A.; Karplus, M. *Nat. Struct. Biol*. **2000**, 7, 34−38.

(27) At very low friction or very high barrier frequencies ($\gamma \ll \omega_B$) eq 10 gives the transition state result $k_{TST} = (\omega_A/2\pi) \exp(-E_0/k_BT)$. However, as $\gamma \rightarrow 0$, as in a gas at low pressure, collisions are too infrequent to constantly supply the transition state with energized molecules, and eq 9 which assumes Brownian motion is no longer valid. In this low friction (inertial) limit Kramers showed that the rate increases with increasing friction. Approximate expressions connecting the high and low friction regimes have been developed (Skinner, J. L.; Wolynes, P. G. *J. Chem. Phys.* **1978**, *69*, 2143-2150).

(28) Lee, M.; Bain, A. J.; McCarthy, P. J.; Han, C. H.; Haseltine, J. N.; Smith, A. B.; Hochstrasser, R. M. *J. Chem. Phys*. **1986**, *85*, 4341−4347.

(29) Barshtein, G.; Almagor, A.; Yedgar, S.; Gavish, B. *Phys. Rev. E* **1995**, 52, 555−557.

(30) Klimov, D. K.; Thirumalai, D. *Phys. Rev. Lett*. **1997**. 79, 317−320.

(31) Loncharich, R. J.; Brooks B. R.; Pastor R. W. *Biopolymers* **1992**, 32, 523−535.

(32) Bagchi, B.; Oxtoby, D. W. *J. Chem. Phys.* **1983**, *78*, 2735−2741. Murarka, R. K.; Bhattacharyya, S.; Biswas, R.; Bagchi, B. *J. Chem. Phys*. **1999**, *110*, 7365−7375.

(33) Vauthey, E. *Chem. Phys*. **1995**, *196*, 569−582.

(34) Brooks, B. R.; Bruccoleri, R.; Olafson, B.; States, D.; Swaminathan, S.; Karplus, M. *J. Comput. Chem.* **1983**, *4*, 187−217.